PERGAMON

Atmospheric Environment 35 (2001) 2395–2404

ATMOSPHERIC ENVIRONMENT

www.elsevier.com/locate/atmosenv

Aircraft observations of aerosols, O_3 and NO_y in a nighttime urban plume

Carl M. Berkowitz*, Rahul A. Zaveri, Xindi Bian, Shiyuan Zhong, Robert S. Disselkamp, Nels S. Laulainen, Elaine G. Chapman

Pacific Northwest National Laboratory, MSIN K9-30, P.O. 999, Richland, WA 99352, USA

Received 24 March 2000; received in revised form 15 October 2000; accepted 30 October 2000

Abstract

Nighttime measurements of aerosol surface area, O_3, NO_y and moisture were made downwind of Portland, Oregon, as part of a study to characterize the chemistry in a nocturnal urban plume. Air parcels sampled within the urban plume soon after sunset had positive correlations between O_3, relative humidity, NO_y and aerosol number density. However, the air parcels sampled within the urban plume just before dawn had O_3 mixing ratios that were highly anti-correlated with aerosol number density, NO_y and relative humidity. Back-trajectories from a mesoscale model show that both the post-sunset and pre-dawn parcels came from a common maritime source to the northwest of Portland. The pre-dawn parcels with strong anti-correlations passed directly over Portland in contrast to the other parcels that were found to pass west of Portland. Several gas-phase mechanisms and a heterogeneous mechanism involving the loss of O_3 to the aerosol surface, are examined to explain the observed depletion in O_3 within the pre-dawn parcels that had passed over Portland. Published by Elsevier Science Ltd.

Keywords: Ozone; Aerosols; Heterogeneous chemistry; Nighttime chemistry; Urban plume; Air pollution

1. Introduction

Homogeneous and heterogeneous chemical processes in the lower troposphere at night have long been recognized to have an uncertainty greater than their daytime counterparts. These uncertainties stem from several considerations. First, although heterogeneous processes of reactive nitrogen compounds, NO_y (which in the troposphere consists primarily of NO, NO_2, NO_3, N_2O_5, HNO_3, peroxyacetyl nitrate (PAN), other organic nitrates and aerosol nitrate), are thought to play a central role in nighttime chemistry, detailed kinetic information about these reactions is lacking. Second, model descriptions of aerosols and reactive trace gases at night are highly uncertain due to a paucity of observations. There are simply very few measurements of NO_y, aerosols or O_3 aloft at night.

In contrast to the paucity of observations, there have been a number of theoretical studies to investigate potential aerosol/oxidant interactions. Dentener and Crutzen (1993), Zhang et al. (1994) and Jacob (2000) have postulated that aerosols can affect atmospheric processes by providing surface area on which trace gases can adsorb and upon which further gas/solid reactions can proceed. The addition of heterogeneous reactions of N_2O_5 and NO_3 on sulfate aerosols decreased simulated O_3 concentrations by 25% in a three-dimensional global tropospheric model (Dentener and Crutzen, 1993). In related work, Dentener et al. (1996) studied the role of aerosols as reaction sites and carriers of condensed and sorbed species. By employing a pseudo-first-order rate coefficient and size-dependent mass transfer coefficients, they calculated O_3 losses due to uptake on mineral aerosols of up to 10%. In a more recent modeling study, de Reus et al. (2000) found a heterogeneous O_3 loss rate on dust aerosols of ~ 4 ppb day^{-1} during the ACE-2 field campaign.

* Corresponding author. Tel.: +1-509-372-6183; fax: +1-509-372-6168.

E-mail address: carl.berkowitz@pnl.gov (C.M. Berkowitz).

1352-2310/01/$ - see front matter Published by Elsevier Science Ltd.
PII: S1352-2310(00)00521-5

This paper presents a set of nighttime air chemistry observations made during aircraft sampling at the top of the residual mixed layer within and adjacent to the urban plume downwind of Portland, Oregon. We begin by describing the flight patterns and instruments, and discuss the meteorological conditions that existed during the flights. We then present measurements that help distinguish background air from the urban plume and note a strong anti-correlation between aerosol number density and O_3 concentration, and between NO_y and O_3 concentrations in air parcels that passed directly over the Portland metropolitan area. This anti-correlation was not observed in air parcels that passed to the west of Portland. We conclude by considering several homogeneous (gas-phase only) mechanisms and a heterogeneous mechanism (gas–aerosol) as potential explanations for the observed anti-correlation between the aerosol, NO_y and O_3.

2. Flight patterns, instrumentation and meteorology

Two flights by the US Department of Energy's (DOE's) Grumman Gulfstream-I (G-1) aircraft, were flown downwind of Portland, Oregon on the evening of 1 September 1998 ('Flight A') and early morning of 2 September ('Flight B'). Each flight consisted of two 'butterfly' patterns at constant altitudes of 900 and 1200 m above mean sea level (msl), as illustrated in Figs. 1 and 2. This pattern was selected to optimize the likelihood of the aircraft encountering the urban plume during forecast conditions of light winds. As will be shown later, the selected altitudes are characteristic of the top of the residual mixed layer over Portland. Also shown in these figures are identifying letters, 'A', 'B', 'C' and 'D' to identify positions and times in subsequent figures. The subscripts (e.g., 'B_L' or 'B_U') refer to the lower or upper altitude segments of the flights, respectively. All flights were made over roughly the same geographical area. Sunset occurred at about 02:40 UTC, and Flights A and B began at approximately 05:00 UTC and 10:00 UTC, respectively. UTC = Pacific Standard Time (PST) + 8 h (e.g., 05:00 UTC = 9 PM PST). The duration of each flight was about 1.5 h.

The G-1 flew with its standard instrument package (Spicer et al., 1994). This package includes a PMS PCASP-100x optical light scattering system mounted externally to the aircraft to measure aerosol number density at 1-s intervals over 15 size channels. The mean diameters associated with these channels are 0.12, 0.14, 0.17, 0.20, 0.25, 0.31, 0.40, 0.54, 0.76, 0.95, 1.20, 1.32, 1.75, 2.25, and 2.75 μm. Mean diameters listed for the first 11 channels were corrected to reflect optically equivalent ambient particle diameters relative to calibration with polystyrene latex spheres using the method of Stolzenburg et al. (1998). Aerosol surface area was calculated using the 10-s average PCASP aerosol number density

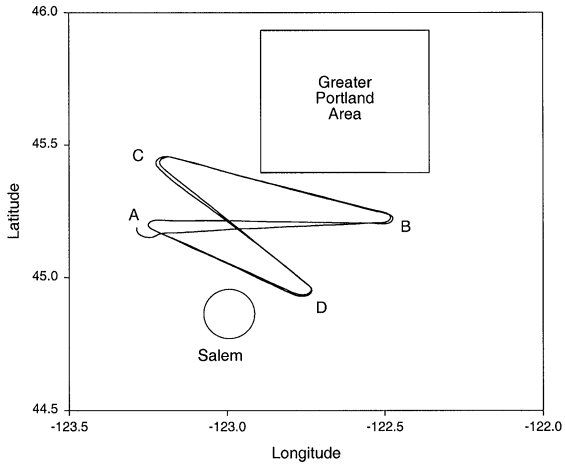

Fig. 1. "Butterfly" flight pattern made during Flight B. Letters are used to identify corresponding points shown in Fig. 2. The outline showing the Greater Portland Area and Salem are based on the National Oceanic and Atmospheric Administration aeronautical charts (1987).

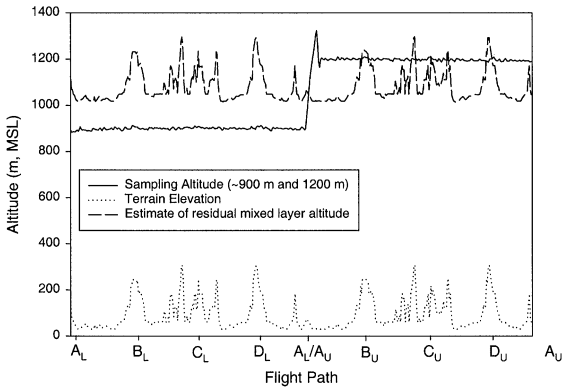

Fig. 2. Sampling altitude and estimate of the altitude of the residual mixed layer along the flight path. Also shown is the terrain elevation over which sampling took place. Letters correspond to those in Fig. 1, with subscripts referring to the lower (e.g., B_L) or upper (e.g., B_U) transects.

data and mean channel diameters. A TSI 3010 condensation particle counter (CPC) was used to measure total aerosol number density for particles larger than 0.01 μm. A three wavelength (450, 550, 700 nm) integrating nephelometer (TSI model 3573) and a Radiance Research particle soot absorption photometer were used to measure light scattering and light absorption coefficients, respectively. Relative humidity was computed from measurements of the dry air temperature (platinum resistance thermometer-Rosemount 510BF probe) and dewpoint temperature (chilled mirror hygrometer-General Eastern 1011B). O_3 was measured using a TECO 49 UV-absorption system and total NO_y measured with a Teco Model

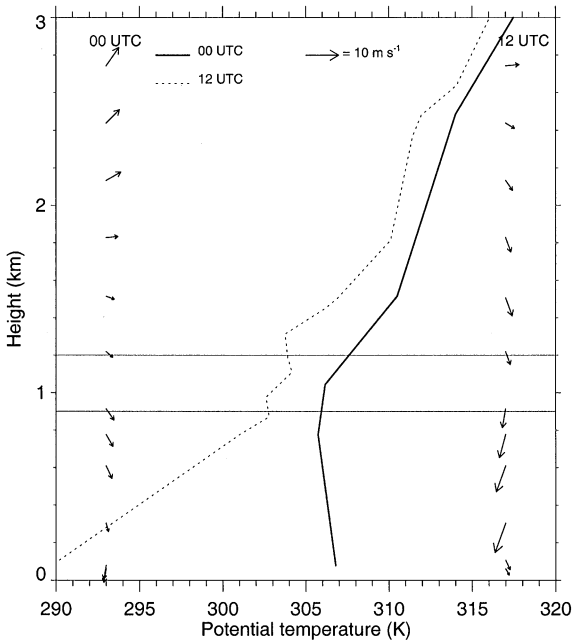

Fig. 3. Potential temperature and wind soundings at 00:00 UTC and 12:00 UTC on 1 September over Salem, OR. The aircraft sampling was done at altitudes indicated by the thin horizontal lines. Solid line shows 00 UTC sounding; dashed line shows 12 UTC sounding.

42S chemiluminescence system having a range, when corrected for other nitrogen species, of 0.3–200 ppb (Kelly et al., 1990).

During the flights of 1 September 1998 a surface thermal low extended inland from Medford, in south-central Oregon, to Portland, with an anticyclonic system building from the southwest along the West Coast of North America. The National Weather Service radiosonde at Salem, Oregon, reported northerly winds between 1 and $2\,\mathrm{m\,s^{-1}}$ at the sampling altitude (Fig. 3). The 00:00 UTC sounding suggests that the height of the mixed layer during the previous afternoon reached over 1000 m in this region. We estimated the height of the daytime mixed layer using the entrainment model of Stull (1988), with the friction velocity, and θ_* and the surface friction temperature scale from planetary boundary layer similarity theory (Businger et al., 1971; Bian et al., 1992). Assuming the mixing layer levelness index (Stull, 1992) is unity, we then estimated the height of the residual mixing layer to be $988\,\mathrm{m} + z_t$, where z_t is the local terrain height. The results of these calculations, shown in Fig. 2, suggest that the G-1 was near the top of the residual layer during the flight.

3. Results and discussion

Fig. 4a shows a time series of O_3, relative humidity (RH), NO_y and CPC aerosol number concentration for the flight made shortly after sunset ('Flight A'). The linear correlation coefficients, R, between these measurements was $> +0.50$, consistent with the visually apparent correlation seen in the vicinity of points A, B and D, south of Portland. A high correlation would be expected among species having a common origin within the daytime urban boundary layer. Observations in the vicinity of Point C, west of Portland, showed a negative or insignificant correlation between O_3 and species having an origin in the urban boundary layer, as would be expected for clean background air. The air mass at Point C also had relatively low levels of NO_y and CPC aerosol number concentrations relative to the levels observed in the rest of the air masses sampled along the flight path.

Fig. 4b shows the corresponding time series taken during Flight B. The NO_y mixing ratios and CPC aerosol number concentration were again strongly correlated with each other ($R \geqslant +0.9$) in the vicinity of B_L, D_L and B_U. However, O_3 was strongly anti-correlated with NO_y ($R \leqslant -0.87$) and CPC aerosol number concentration ($R \leqslant -0.94$). The CPC, NO_y and RH values were also higher at these points than the values measured in the surrounding areas. In contrast, the observations near Points A and C, to the west of Portland showed a negative or insignificant correlation between these measurements. These points were also characterized by lower RH, O_3, NO_y and CPC aerosol number concentrations, as would be associated with clean background air.

Air sampled near points B_L, D_L, B_U and D_U during Flight B had other unique characteristics relative to measurements made near other points. Although no specific measurements of aerosol mass concentration or chemical composition were available, the aerosol light scattering coefficient has been shown to be proportional to fine particle mass via the extinction efficiency (Charlson et al., 1999 and references therein), while the light absorption coefficient can provide a measure of black carbon mass. The single scattering albedo, ω_o, was calculated in the standard manner as the ratio of total light scattering to the total light extinction (scatter plus absorption). Values of ω_o between 0.8 and 0.9 at and in the immediate vicinity of points B_L, D_L, B_U and D_U (Fig. 4c) suggests that parcels associated with these intervals contained some aerosol absorptive component, perhaps carbonaceous material. Values of ω_o are lower (0.6–0.7) near points A and C, perhaps due to strongly absorbing biogenic carbonaceous aerosols. The overlaying plot of mean number diameter ($\sum_i N_i D_{p,i} / \sum_i N_i$, where N_i and $D_{p,i}$ are the observed number density in PCASP bin i having mean size D_i) in Fig. 4c clearly shows that the average size of aerosols sampled at points A and C is much smaller than the size of particles measured to the east of these locations. Interestingly, the average number diameter profile is also strongly correlated with the O_3 concentration time series shown in Fig. 4b.

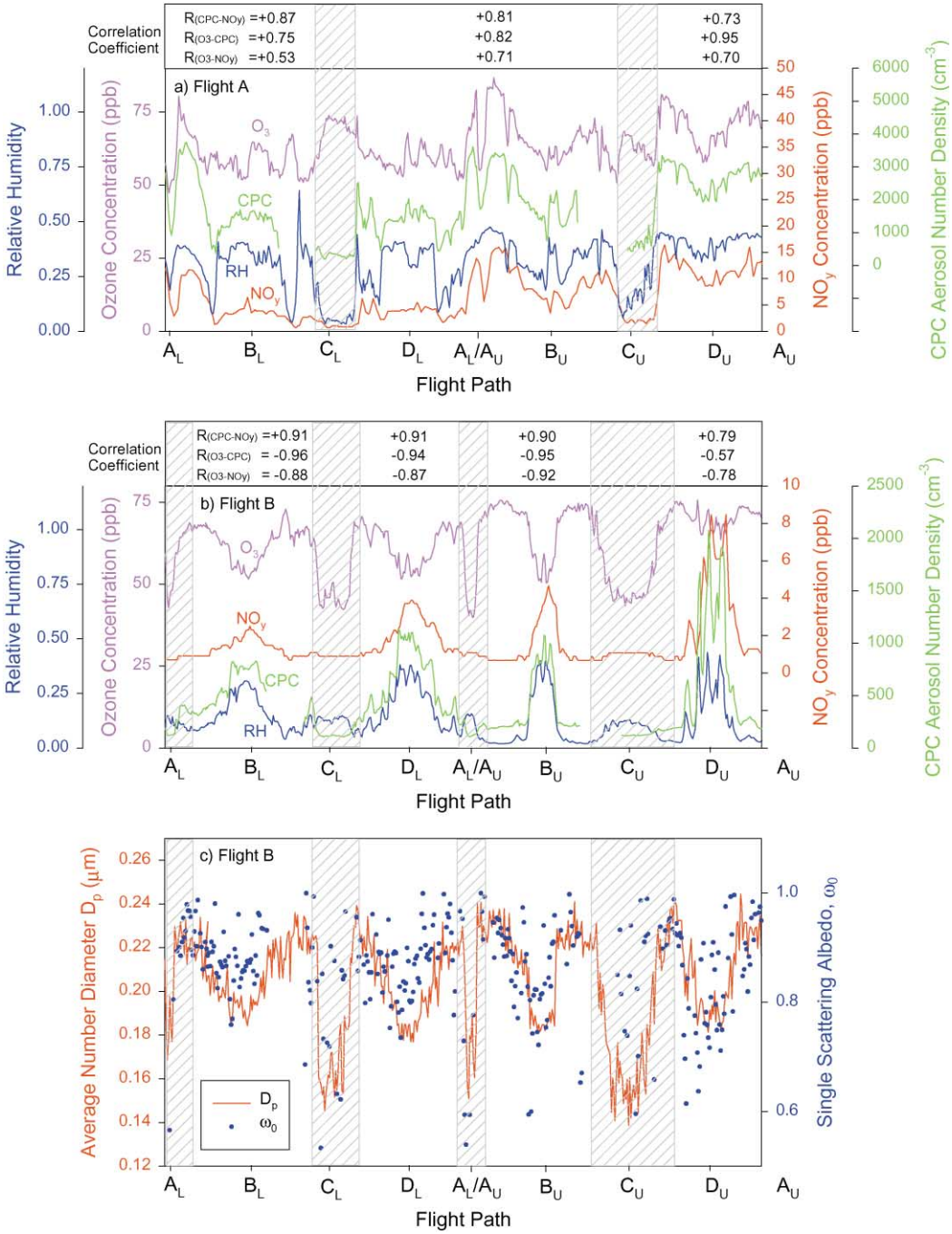

Fig. 4. (a) Relative humidity, O_3, NO_y and CPC aerosol number density along the flight path during Flight A (05:00 UTC – 06:30 UTC). Also shown are the correlations coefficients for CPC–NO_y, O_3–CPC, and O_3–NO_y profiles Letters (A_L, B_L, etc.) identify the geographical position of the aircraft, as shown in Figs. 1 and 2. Shaded vertical areas mark the extent of clean background air mass. (b) Same as (a), but for Flight B (10:00 UTC – 11:30 UTC). (c) Average number diameter and single scattering albedo along the flight path during Flight B.

These differences suggest that the air mass at points A and C is quite different than the air mass near points B and D, 10–20 km to the east. This distinction is further supported by the spatial distribution of total PCASP aerosol number density along the flight path (Fig. 5). We have used the PCASP observations to define regions

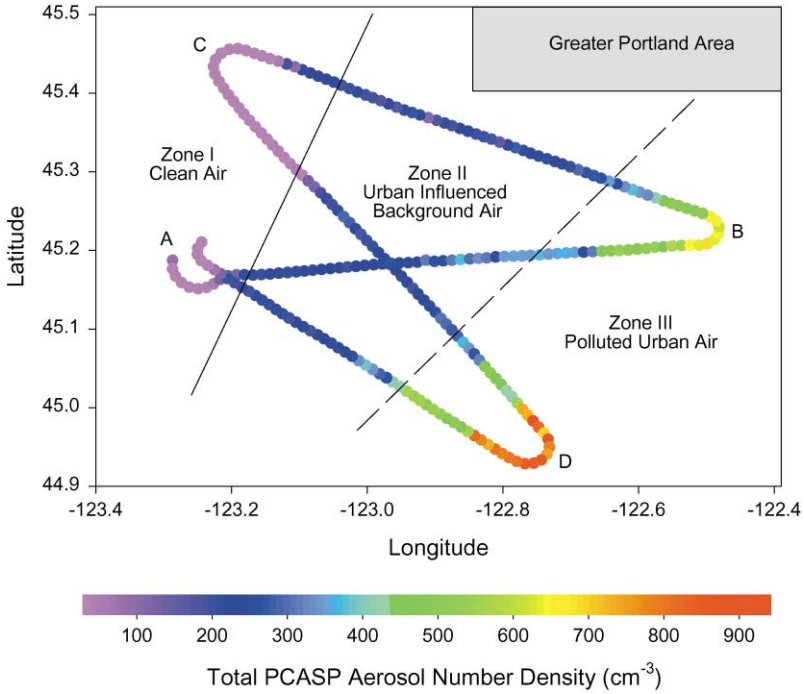

Fig. 5. Spatial distribution of the total PCASP aerosol number density, and arbitrary demarcations of the different types of air masses.

with clean background air (Zone I), regions that are a mix of urban and background air (Zone II) and a region that is predominantly polluted urban air (Zone III).

Recognizing that the properties, chemical or physical, of an air parcel are a function of its history, an analysis was made of the vertical mixing and back trajectories of air sampled during the late night sampling mission (Flight B). A Lagrangian Particle Dispersion Model (LPDM) (Fast, 1995; Fast and Zhong, 1998) was used to identify the origin of the air passing the sampling locations at the time of the sampling. The LPDM was driven by wind fields simulated by Regional Atmospheric Modeling System (RAMS, Pielke et al., 1992) and employed three nested grids at 32, 8, and 2 km horizontal grid resolution and 42 vertical levels with 25 placed in the lowest 3 km to resolve the details in the vertical boundary layer structures. The outer grid encompassed the Western Pacific Ocean and the entire Pacific Northwest while the inner grid covered southwestern Washington and northwestern Oregon. The simulation was initialized with the National Center for Environmental Prediction Aviation model analysis at 00:00 UTC 1 September and ended at 12:00 UTC 2 September. The simulated temperature structures and wind speeds and directions compared well with the soundings at Salem in southwest Oregon. Good agreement was also found between simulated near-surface winds and temperatures and those measured by several surface stations in western and central Oregon.

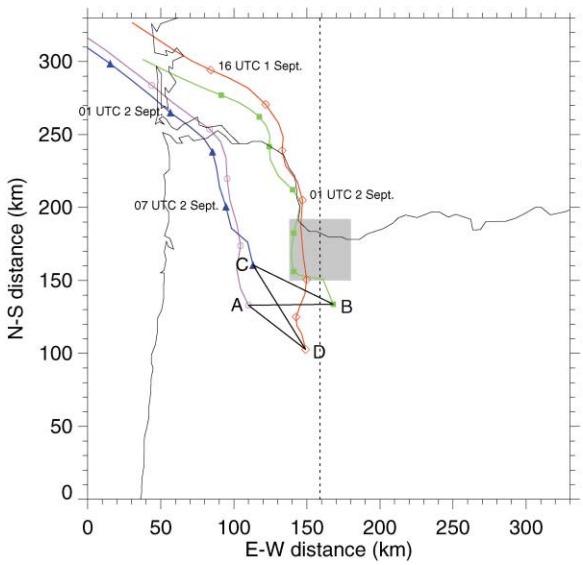

Fig. 6. Representative back trajectories of particles near the four sampling points along the lower flight segment at 10:00 UTC, 2 September. Each trajectory segment represents 3 h duration. The N–S dashed line indicates the position for the vertical cross section in Fig. 7.

The mean wind fields from the RAMS simulation were used to describe the transport of particles backward from the time of their release. Fig. 6 shows representative back trajectories starting at points A_L, B_L, C_L, and D_L, at

10:00 UTC. While the air sampled at all four points emanated from a common region off the Washington coast northwest of Portland, air arriving at points A and C remained west of Portland, whereas air arriving at B and D passed directly over Portland before sunset. Furthermore, the air arriving at points B and D took about 1 day to reach the sampling domain after crossing the coastline while the air arriving at points A and C took only 12 h. Thus, the air sampled at Points A–C and B–D, probably had similar chemical and aerosol characteristics when upwind of Portland, but encountered significantly different chemical environments as they passed through or near Portland prior to reaching the sampling domain. Although we did not measure the O_3 concentration immediately upwind of the Greater Portland area, the time series in Fig. 4b suggests that this background O_3 concentration was $\sim$75 ppb (the highest levels observed in Zone II), which is markedly different from the $\sim$55 ppb levels observed in Zone I. Thus, the anti-correlations between O_3 and aerosol, and O_3 and NO_y concentrations noted in Zones II and III appear to be associated with the passage of air over the urban area.

A second set of LPDM runs were made to evaluate the extent to which nocturnal vertical mixing of surface layer air upwards had on the aircraft measurements. Simulated particles were released near the surface from the Greater Portland area between 08:00 UTC (1:400 PST on 1 September) to 20:00 UTC (04:00 PST) the next morning. Particles released prior to sunset 10:40 UTC (18:40 PST) were assumed to characterize the position of the daytime plume. Those released later were assumed to characterize the position of the nighttime plume. For these simulations particles were tracked forward in time as they were advected south from the Portland area by the mean + turbulent motions. The sub-grid scale turbulent velocities were computed by solving the Langevin equation with a Markov chain formulation (Legg and Raupach, 1982) that is based on the Thomson formulation for the turbulent vertical velocity component (Hurley and Physick, 1991).

Fig. 7 shows both the daytime and nighttime particle distribution at 10:00 UTC, 2 September projected along a north-to-south vertical cross section that passes through the center of the Greater Portland area (shown by the dotted line shown in Fig. 6). Particles released in the afternoon were buoyed upward by vigorous vertical turbulent mixing to near 1500 m while being carried downwind towards the sampling area south of Portland. In contrast, particles released at night were confined to the lowest levels as a result of the stable nocturnal stratification and did not reach the aircraft sampling altitudes.

A consequence of the results described above is that it is unlikely that the observed anti-correlation can be explained via the upward mixing of boundary-layer air having high concentration of sub-micron aerosols and low O_3 mixing ratios. Low O_3 mixing ratios are commonly observed near the surface at night, and are explained via the well-known titration of O_3 by NO. However, there are other difficulties of a

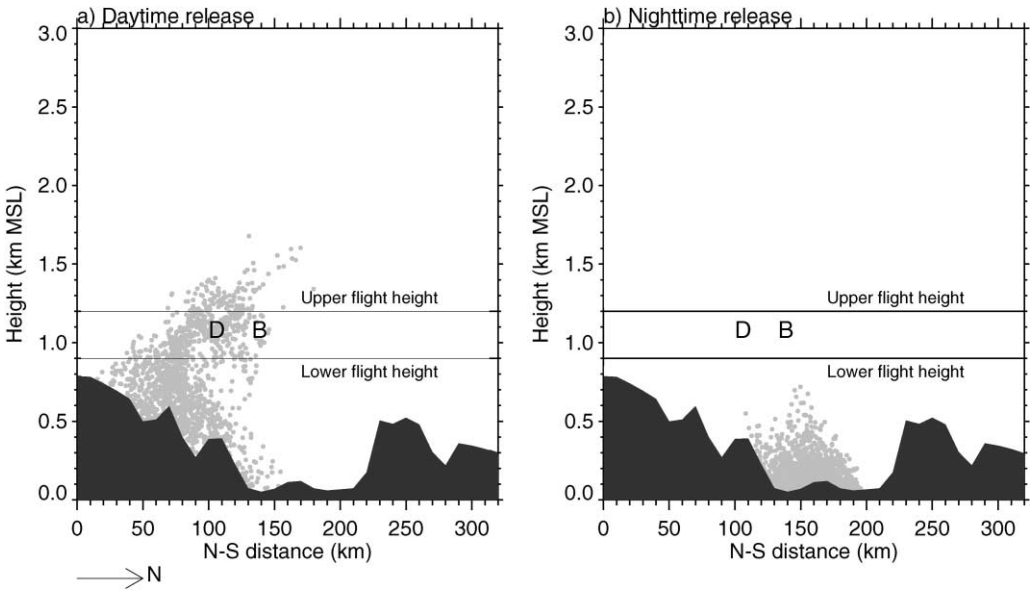

Fig. 7. Vertical distribution of particles on a N–S vertical cross section through the center of the Greater Portland area between points B and D (dashed line in Fig. 7) at 10:00 UTC, 2 September. All particles bounded by point D to the west and B to the east are projected to this cross section. Panel (a) shows particles released before sunset at 02:40 UTC and panel (b) shows particles released after sunset.

non-meteorological nature that the $NO + O_3$ model must explain, as will now be discussed.

4. Two sets of hypothesis to explain the observed anti-correlation

4.1. Homogeneous gas-phase chemistry

The homogeneous gas-phase removal of O_3 through reaction with NO is an obvious candidate reaction to explain any observed depletion of O_3 at night. NO levels during Flight B were always at or below the detection limit of 0.20 ppb even though total NO_y levels varied between 0.7 and 8.5 ppb. It is possible that the removal of O_3 by freshly emitted NO occurred within a boundary layer source region common to NO, O_3 and combustion-generated sub-micron aerosols. The $NO + O_3$ reaction could eventually result in low NO, low O_3 and relatively high aerosol concentrations. Results from the LPDM study imply very little exchange of surface air with air at the sampling height of the G-1, consistent with the low concentrations of NO emitted near the surface.

To quantify the maximum possible loss of O_3 by NO_x, we assumed that all the measured NO_y was emitted as NO in an air mass passing over the Greater Portland area at sunset, containing ~ 75 ppb of O_3. The nighttime chemistry of NO_x and O_3 was simulated using a box-model with the chemical mechanism of Zaveri and Peters (1999). The NO concentrations were initialized using the observed NO_y concentrations along the flight path, the O_3 concentrations were set to 75 ppb and the temperature kept constant at 298 K. Fig. 8 shows the simulated O_3 time series 7 h from sunset, corresponding to the time of Flight B. Although the simulated O_3 values at point D_U are in good agreement with the observations, these model calculations show that the maximum NO levels are far below those needed to produce the observed 15–20 ppb O_3 decreases at points B_L, D_L and B_U.

It is possible that the air masses at these points may have had much higher initial NO levels which were converted into soluble HNO_3 and lost to liquid water present on the aerosols. This process would have resulted in NO_y levels that underestimated the total possible NO used in the above model calculations. This phenomenon cannot be completely ruled out. However, it seems unlikely since the observed relative humidity values were too low (10–40%) for enough aerosol liquid water to be present to absorb the 15–20 ppb of HNO_3 at 298 K needed to explain the O_3 loss. It is well known that the presence of NH_3 can lead to the formation of solid NH_4NO_3 at RH levels below 62% (Seinfeld and Pandis, 1998 and references therein). Assuming that all the observed gas-phase NO_y was HNO_3, then for it to exist in equilibrium with solid NH_4NO_3 at 298 K, would require $\sim$30–15 ppb NH_3 in the gas-phase at points B_L and B_U, respectively. Although we did not measure NH_3, it seems unlikely that levels this high would be present (Finlayson-Pitts and Pitts, 2000).

A third possible source for homogeneous O_3 depletion could involve O_3 and reactive alkenes in polluted air masses after sunset. However, at least 15–20 ppb of reactive alkenes (or olefinic bonds) are needed to explain the observed O_3 deficits. While we do not have measurements of any organic species, these values seem too high for a moderately polluted air mass (Chameides et al., 1992).

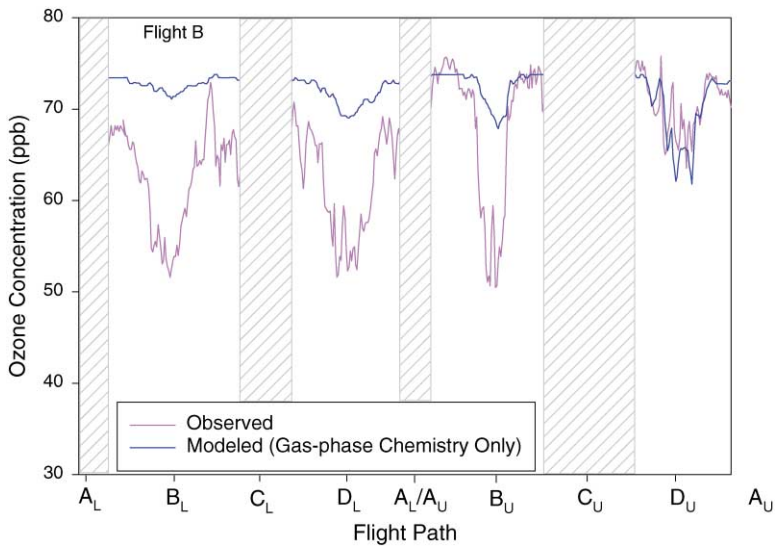

Fig. 8. Observed and modeled O_3 concentrations using only gas-phase chemistry.

4.2. Heterogeneous chemistry

We now consider the possibility that the elevated aerosol number density, and hence the aerosol surface area, observed in the air parcels that passed over Portland was related to the observed depletion in O_3. To evaluate this hypothesis we assume O_3 reacts irreversibly on aerosol surfaces. The loss per aerosol particle, J_c (mol^{-1} particle^{-1}) is described by Maxwell's equation for the flow towards the particle applicable in a continuous medium (Seinfeld and Pandis, 1998):

$$J_c = 4\pi R_p D_g (c_\infty - c_s), \quad (1)$$

where R_p is the aerosol radius (cm), D_g is the diffusivity of O_3 in air ($cm^2\,s^{-1}$) and c_∞ and c_s are the concentrations ($mol\,cm^{-3}$) in the atmosphere and at the aerosol surface. Assuming $c_s = 0$ the expected depletion of O_3 associated with the total number of particles can then be described by the first-order loss process,

$$\partial[O_3]/\partial t = -\sum_i J_{c,i} N_i f(Kn_i). \quad (2)$$

Here the summation is performed over PCASP aerosol bins i; N_i is the aerosol number density in ith bin; $f(Kn_i)$ is a dimensionless correction term to be applied when the mean free path of the diffusing vapor molecule (λ) is comparable to the mean bin diameter, $D_{p,i}$, of the aerosols. The Knudsen Number, $Kn_i = 2\lambda/D_{p,i}$, for this situation is of order unity since $\lambda \sim 1.5\,\mu m$ for O_3, hence the need to consider this transition regime where $\lambda \sim D_{p,i}$. This correction is taken from Fuchs and Sutugin (1971):

$$f(Kn) = 0.75\alpha(1 + Kn)/(Kn^2 + Kn + 0.283Kn\alpha + 0.75\alpha), \quad (3)$$

where α is a dimensionless constant accommodation coefficient. For reasons discussed below, α was set to 1.2×10^{-3}. This first-order heterogeneous reaction was added to the box model described in the preceding section. As shown in Fig. 9 this simple model reproduces the observed O_3 minimum to within a few ppb.

To evaluate the role of local moisture in this loss process, the accommodation coefficient was next defined to be a linear function of the observed relative humidity, $\alpha = RH\alpha_1 + \alpha_0$, By setting $\alpha_1 = 4 \times 10^{-3}$ and $\alpha_0 = 1 \times 10^{-7}$, this model reproduced not only the observed minimum O_3 but also the observed values pre- and proceeding the minimum. Indeed, the resulting modeled time series is difficult to distinguish near points B_L, D_L and B_U from the observed time series (Fig. 9). It thus appears that water vapor, and thus surface moisture, may play an important, though not yet understood, role in explaining these observations.

The performance of this simple uptake model is predicated on an accommodation coefficient for O_3 on aerosol of 10^{-3}. Reported reaction probabilities of O_3 on aerosol surfaces range from 10^{-3} to less than 10^{-7} (Fendel et al., 1995; Smith and Chughtai, 1996; Rogaski et al., 1997; de Gouw and Lovejoy, 1998; Kamm et al., 1999; Disselkamp et al., 2000). These differences may be due to the experimental technique employed (Knudsen cell, aerosol flow tube, or static chamber apparatus),

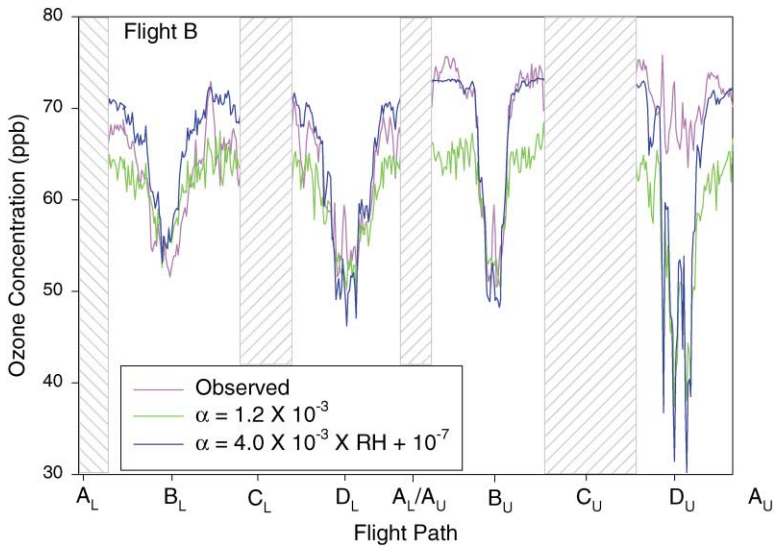

Fig. 9. Observed and modeled O_3 concentrations using gas-phase chemistry and heterogeneous chemistry. The green line shows model results using a constant accommodation coefficient. The blue line shows results using an accommodation coefficient that is a function of moisture (see text).

materials studied, or material passivation arising from prolonged exposure to O_3 (see Disselkamp et al., 2000 and references therein). Furthermore, most or all of the laboratory experiments have been conducted in extremely dry air where as ambient atmospheric aerosols would most likely have some moisture present on the surface, even at 10–40% RH, which may play an important role in surface reactions as suggested by our model analyses. And while the optical absorption properties reported here suggest an organic carbonaceous material, the specific material is unknown, as is the actual ozone–aerosol loss mechanism.

5. Final remarks and future directions

Although our measurements provide only circumstantial evidence for heterogeneous O_3 depletion in a nighttime urban plume, the implications of such a process on air quality modeling could be significant. The heterogeneous loss of O_3 on aerosols would also be important during the daytime even though we would not expect to find the strong anti-correlations reported due to competing changes associated with vigorous photochemistry, transport (vertical and horizontal), surface removal via dry deposition, and the addition of fresh emissions of both gaseous species and aerosols.

Three observations should be included in future nighttime urban plume studies in addition to those described in this paper. First, measurements within an air mass should be made before, during and after air passage over an urban region. These observations would provide the initial chemical/aerosol conditions and intermediate values needed for hypothesis evaluation. Aerosol composition will be a critical factor in elucidating the chemistry associated with O_3 (or oxidant) loss processes. And finally, real-time measurements are needed of HONO, HNO_3, NO_2, NO, HCHO, alkenes, isoprene, monoterpenes, and other trace gas species thought to be associated with trace gas/aerosol chemistry.

Acknowledgements

We gratefully acknowledge the flying skills of Bob Hannigan and Dick Hone who translated our scientific needs into safe flight patterns with the G-1; Chet Spicer and Bob Plastridge of Battelle Columbus Laboratory for making the NO_y measurements; John Hubbe and Vic Morris for reliable acquisition and reduction of onboard data; Rich Barchet of the DOE Research Aviation Facility for taking care of innumerable administrative issues; the Federal Aviation Agency, Portland office, for providing us with radar coverage during the nighttime flights; and the US. Department of Energy's Atmospheric Chemistry Program for providing the resources and support necessary to make these measurements. We are also grateful to the anonymous reviewers for a thorough review of an earlier version of the manuscript. Pacific Northwest National Laboratory is operated for the US Department of Energy by Battelle Memorial Institute under contract DE-AC06-76RLO 1830.

References

Bian, X., Takle, E.S., Zhong, S.A., 1992. Theoretical study of the flux-profile relationships: extension of the KEYPS equation to the tower layer. Proceedings of the 10th Symposium on Turbulence and Diffusion, September 29–October 2, American Meteorological Society, Portland, OR.

Businger, A.K., Wyngaard, J.C., Izmi, Y., Bradley, E.F., 1971. Flux-profile relations in the atmospheric surface layer. Journal of Atmospheric Science 28, 181–189.

Chameides, W.L., Fehsenfeld, F., Rodgers, M.O., Cardelino, C., Martinez, J., Parrish, D., Lonneman, W., Lawson, D.R., Rasmussen, R.A., Zimmerman, P., Greenberg, J., Middleton, P., Wang, T., 1992. Ozone precursor relationships in the ambient atmosphere. Journal of Geophysical Research 97, 6037–6055.

Charlson, R.J., Anderson, T.L., Rodhe, H., 1999. Direct climate forcing by anthropogenic aerosols: quantifying the link between radiation and sulfate models. Beiträge zur Physik der Atmosphäre 72, 79–94.

de Gouw, J.A., Lovejoy, E.R., 1998. Reactive uptake of ozone by liquid organic compounds. Geophysical Research Letters 25, 931–934.

de Reus, M., Dentener, F., Thomas, A., Borrmann, S., Ström, J., Lelieveld, J., 2000. Airborne observations of dust aerosol over the North Atlantic Ocean during ACE 2: indications of heterogeneous ozone destruction. Journal of Geophysical Research 105, 15263–15276.

Dentener, F.J., Carmichael, G.R., Zhang, Y., Lelieveld, J., Crutzen, P.J., 1996. Role of mineral aerosol as a reactive surface in the global troposphere. Journal of Geophysical Research 101, 22869–22889.

Dentener, F.J., Crutzen, P.J., 1993. Reaction of N_2O_5 on tropospheric aerosols: impact on the global distributions of NO_x, O_3 and OH. Journal of Geophysical Research 98, 7149–7163.

Disselkamp, R.S., Carpenter, M.A., Cowin, J.P., Berkowitz, C.M., Chapman, E.G., Zaveri, R.A., Laulainen, N.S., 2000. Ozone loss on atmospheric soot aerosols. Journal of Geophysical Research 105, 9767–9772.

Fast, J.D., 1995. Mesoscale modeling in areas of highly complex terrain. Journal of Applied Meteorology 34, 2762–2782.

Fast, J.D., Zhong, S., 1998. Meteorological factors associated with inhomogeneous ozone concentrations within the Mexico City basin. Journal of Geophysical Research 103, 18927–18946.

Fendel, W., Matter, D., Burtscher, H., Schmidt-Ott, A., 1995. Interaction between carbon or iron aerosol particles and ozone. Atmospheric Environment 29, 967–973.

Finlayson-Pitts, Barbara J., Pitts Jr., J.N., 2000. Chemistry of the Upper and Lower Atmosphere, Theory, Experiments, and Applications.. Academic Press, San Diego, CA.

Fuchs, N.A., Sutugin, A.G., 1971. High dispersed aerosols. In: Hidy, G.M., Brock, J.R. (Eds.), Topics in Current Aerosol Research (Part 2). Pergamon, New York, pp. 1–200.

Hurley, P., Physick, W., 1991. A Lagrangian particle model of fumigation by breakdown of the nocturnal inversion. Atmospheric Environment 25, 1313–1325.

Jacob, D.J., 2000. Heterogeneous chemistry and tropospheric ozone. Atmospheric Environment 34, 2131–2159.

Kamm, S., Möhler, O., Naumann, K.-H., Saathoff, H., Schurath, U., 1999. The heterogeneous reaction of ozone with soot aerosol. Atmospheric Environment 33, 4651–4661.

Kelly, T.J., Spicer, C.W., Ward, G.F., 1990. An assessment of the luminol chemiluminescence technique for measurement of NO_2 in ambient air. Atmospheric Environment 24A, 2397–2403.

Legg, B.J., Raupach, M.R., 1982. Markov-chain simulation of particle dispersion in inhomogeneous flows: the mean drift velocity induced by a gradient in Eulerian velocity variance. Boundary Layer Meteorology 24, 3–13.

National Oceanic and Atmospheric Administration (NOAA), 1987. Seattle Sectional Aeronautical Chart, US Department of Commerce, Washington DC.

Pielke, R.A., et al., 1992. A comprehensive meteorological modeling system: RAMS. Meteorlogical Atmospheric Physics 49, 69–91.

Rogaski, C.A., Golden, D.M., Williams, L.R., 1997. Reactive uptake and hydration experiments on amorphous carbon treated with NO_2, SO_2, O_3, HNO_3, and H_2SO_4. Geophysical Research Letters 24, 381–384.

Seinfeld, J.H., Pandis, S.N., 1998. Atmospheric Chemistry and Physics from Air Pollution to Climate Change. Wiley, New York.

Smith, D.M., Chughtai, A.R., 1996. Reaction kinetics of ozone at low concentrations with n-hexane soot. Journal of Geophysical Research 101, 19607–19620.

Spicer, C.W., Kenny, D.V., Shaw, W.J., Busness, K.M., Chapman, E.G., 1994. A laboratory in the sky: new frontiers in measurements aloft. Environmental Science and Technology 28, 412A–420A.

Stolzenburg, M., Kreisberd, N., Hering, S., 1998. Atmospheric size distributions measured by differential mobility optical particle size spectrometry. Aerosol Science and Technology 29, 402–418.

Stull, R.B., 1988. An Introduction to Boundary Layer Meteorology. Kluwer Academic Publishers, Dordrecht.

Stull, R.B., 1992. A theory for mixed-layer-top levelness over irregular topography. Proceedings of the 10th Symposium on turbulence and Diffusion, September 29–October 2, American Meteorological Society, Portland, OR.

Zaveri, R.A., Peters, L.K., 1999. A new lumped structure photochemical mechanism for large-scale applications. Journal of Geophysical Research 104, 30387–30415.

Zhang, Y., Sunwoo, Y., Kotamarthi, V., Carmichael, G.R., 1994. Photochemical oxidant processes in the presence of dust: an evaluation of the impact of dust on particulate nitrate and ozone formation. Journal of Applied Meteorology 33, 813–824.